JACS
JOURNAL OF THE AMERICAN CHEMICAL SOCIETY

Article

pubs.acs.org/JACS

A Two-Step Synthetic Strategy toward Monodisperse Colloidal CdSe and CdSe/CdS Core/Shell Nanocrystals

Jianhai Zhou, Chaodan Pu, Tianyu Jiao, Xiaoqi Hou, and Xiaogang Peng*

Center for Chemistry of Novel & High-Performance Materials, Department of Chemistry, Zhejiang University, Hangzhou 310027, P. R. China

Supporting Information

ABSTRACT: CdSe magic-size clusters with close-shell surface and fixed molecular formula are well-known in the size range between ∼1 and 3 nm. By applying high concentration of cadmium alkanoates as ligands, a conventional synthetic system for CdSe nanocrystals was tuned to discriminate completion from initiation of atomic flat facets. This resulted in ∼4−13 nm CdSe nanocrystals with hexahedral shape terminated with low-index facets, namely three (100), one (110), and two (111) facets. These low-symmetry (C_s group with single mirror plane) yet monodisperse hexahedra were found to be persistent not only in a broad size range but also under typical synthetic temperatures for growth of both CdSe and CdS. Atomic motion on the surface of the nanocrystals under enhanced ligand dynamics initiated intraparticle ripening without activating interparticle ripening, which converted the hexahedral nanocrystals to monodisperse spherical ones. This new synthetic strategy rendered optimal color purity of photoluminescence (PL) of the CdSe and CdSe/CdS core/shell nanocrystals, with the ensemble PL peak width comparable with that of a corresponding single dot.

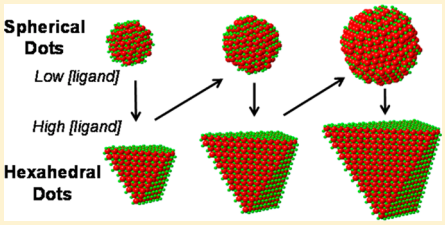

INTRODUCTION

Colloidal semiconductor nanocrystals with their sizes in quantum confinement regime are known as quantum dots.[1] Their size-dependent photoluminescence (PL) and electroluminescence properties, convenient excitation, and solution processability render them as outstanding emissive materials in many applications, such as light-emitting diodes,[2−4] biological labeling/imaging,[5,6] lasers,[7] and single-photon sources.[8] Many of these applications would be greatly benefited by existence of quantum dots with their ensemble PL peak width comparable to that of a single dot. For most developed CdSe and other II−VI semiconductor nanocrystals, strictly monodisperse ones are made available through synthesis of those magic-size clusters with defined molecular formula in the size range between 1 and 3 nm.[9−24] Magic-size clusters of II−VI semiconductors are found to possess interior atomic packing similar to that in bulk zinc-blende structure and be terminated with atomically flat (or faceted) surfaces, which results in extremely sharp UV−vis absorption spectra. Except trap emission, however, CdSe magic size clusters usually do not emit. The PL peak width and absorption spectra of conventional quantum dots produced by the state-of-art synthesis would be comparatively broad.[25,26] For most developed CdSe nanocrystals (>3 nm), the Bawendi's group reported the single-dot PL fwhm (full width at half-maximum) being ∼60−75 meV in average,[27] while ∼80 meV was considered as a narrow fwhm for ensemble PL of CdSe quantum dots.[28]

Formation mechanism of magic-size clusters is largely unknown and, in terms of synthetic strategy, there is little commonality from one work to another.[9−24] Apart from synthesis of magic-size clusters, synthetic strategies for conventional quantum dots can be classified into three main categories. The first category targets rapid nucleation followed by slow growth without Ostwald ripening. This would result in "focusing of size distribution" because the relatively small ones would catch-up by growing faster than the large ones in the solution.[29] The second category relies on a high concentration of nanocrystals, which enables rapid and complete dissolution of relatively small ones in the distribution and slow growth of the relatively large ones.[30−32] The third category is fusion of primary particles in the solution, which might start from either oriented[33] or nonoriented[34] attachment of the primary crystals. For the third category, "intraparticle ripening"[34,35] is often required to smooth the surface of fused nanocrystals to yield nearly monodisperse products. Size distribution of the resulting nanocrystals from all these strategies is often complicated by the morphology of the nanocrystals. For example, it has been widely reported that semiconductor nanocrystals might be faceted to a certain extent, but the faceting has never been as perfect as that of magic-size clusters.[36]

This report describes a two-step strategy to synthesize nearly monodisperse CdSe nanocrystals, whose ensemble PL fwhm is as narrow as that of the corresponding single dot. In the first step, growth conditions were optimized to discriminate completion from initiation of atomically flat facets. Such layer-by-layer growth was known ∼80 years ago for growth of bulk crystals.[37] Layer-by-layer growth in three dimensions developed by this work resulted in monodisperse hexahedra with six fixed facets persistently for a broad size range (>3 nm)

Received: January 20, 2016
Published: May 4, 2016

DOI: 10.1021/jacs.6b00674
J. Am. Chem. Soc. 2016, 138, 6475−6483

for CdSe nanocrystals. In the second step, intraparticle ripening[35] was applied to remove the sharp corners and edges of the hexahedra and converted them to monodisperse spherical ones.

RESULTS AND DISCUSSION

Design of Reaction Scheme. Fully characterized CdSe magic size clusters (~1−3 nm in size) were constructed with zinc-blende cores though their surface might possess slight wurtzite-like reconstruction.[9−24] This motived us to consider zinc-blende CdSe nanocrystals (> ~3 nm) to realize the targeted two-step—layer-by-layer growth followed by intraparticle ripening—synthetic scheme (Figure 1). Dot-shaped

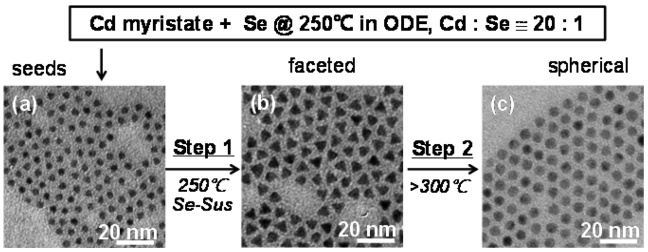

Figure 1. Schematic illustration of the synthetic strategy. Transmission electron microscope (TEM) images were taken using the aliquots taken at different stages. The resulting spherical nanocrystals to the right could be applied as seeds to reinitiate the growth cycle. Se-Sus: Se suspension in octadecene (ODE).

zinc-blende CdSe nanocrystal seeds were synthesized using an approach reported in literature.[38] The spherical nanocrystals obtained at the end of the second step could also be applied as seeds for growth of even large nanocrystals. This means that the growth scheme in Figure 1 could be applied in cycle.

Atomically flat crystal facets of magic-size clusters are saturated with stable ligand coordination,[9,10,12,13,15,18,22−24,39] which should be the necessary structural features for the targeted faceted nanocrystals resulted from the layer-by-layer growth. However, if ligand dynamics—ligands switching between bonding and detaching on the surface of nanocrystals on thermal activation—was not active, growth of nanocrystals would barely take place.[40] These two competitive factors encouraged us to apply an extremely high concentration of Cd alkanoaes as ligands during the first step of the scheme shown in Figure 1, i.e., ~20 times that of the initial Se concentration. Consistent with this hypothesis, results (Figure S1, Supporting Information) confirmed that relative low concentrations of the ligands could not offer good surface passivation under active ligand dynamics under elevated temperatures.

An extremely high concentration of the ligands would result in slow growth onto the seeds due to enhanced diffusion barrier for active monomers onto the nanocrystal surface. This should be beneficial for the targeted layer-by-layer growth, i.e., the first step in the Scheme in Figure 1. However, high concentration of cadmium alkanoates often caused nucleation of new CdSe nanocrystals while the Se precursor was added into the solution. To battle this problem, dropwise addition of Se precursor and a suitable concentration of free fatty acid would be necessary (Figure S2, Supporting Information). Layer-by-layer growth was optimized at ~250 °C but persisted from 240 to ~280 °C (Figure S3, Supporting Information).Temperature up to ≥300 °C was found to yield regular dot-shaped nanocrystals with a relatively broad size/shape distribution (Figure S4, Supporting Information). This was expected as relatively high temperatures would drive ligand dynamics too active to promote the selective layer-by-layer growth.

If the faceted nanocrystals were relatively small in size, the second step in Figure 1 was initiated by simply increasing the reaction temperature to >300 °C. For the faceted nanocrystals with medium sizes, removal of the excess free ligands (Figure S5, Supporting Information) greatly accelerated this conversion step. Conversion of those extremely large ones was further prompted by addition of fatty amines into the reaction solution (see detail below). It was well-known that fatty amine can replace carboxylate ligands under elevated temperatures,[41] and ligand dynamics of fatty amine on the surface of CdSe nanocrystals was active even at room temperature.[40,42]

Layer-by-Layer Growth To Form Faceted Nanocrystals. To illustrate layer-by-layer growth in the current system, temporal shape evolution of the CdSe nanocrystals at the first step was monitored by TEM along with their optical properties (Figure 2). For convenience, all samples related to Figure 2

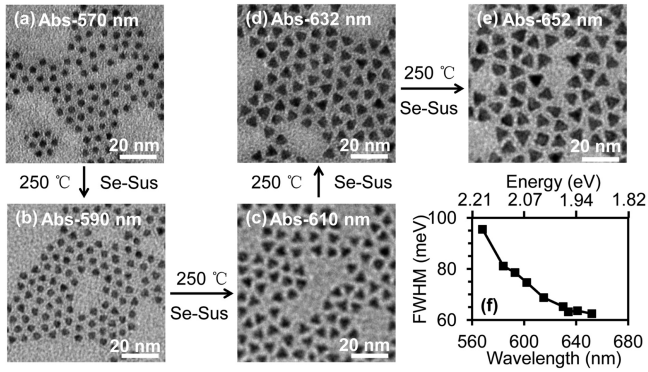

Figure 2. TEM images of seeds (a), intermediate state (b), and the fully faceted nanocrystals with different sizes (c−e) from one reaction. (f) Temporal evolution of PL fwhm of the aliquots taken at different reaction time (top *x*-axis not in linear scale).

were labeled with their corresponding lowest-energy UV−vis peak. The CdSe seeds (Abs-570, Figure 2a) were spherical nanocrystals. Nanocrystals in Figure 2b began to grow corners, but their facets were not fully developed. Nanocrystals in Figure 2c−e appeared to be fully faceted. Persistence of the morphology from Figure 2c to Figure 2e was further conformed under different reaction temperatures and for seeds with different sizes (Figure S3).

Along growth of the faceted nanocrystals, Figure 2f shows that the ensemble PL fwhm decreased greatly in the early stage and gradually reached a plateau. The ensemble PL fwhm of the seeds was ~96 meV, while it was <80 meV for the corresponding single dot in the size range.[27] Conversely, the ensemble PL fwhm of those fully faceted nanocrystals (Figure 2) was in good accordance with that of the corresponding single dots (~55−70 meV in the size range[27]).

Size difference between the seeds and the smallest fully faceted nanocrystals in a given reaction (Figures 2 and S3 (Supporting Information)) corresponded to ~2−3 monolayers of growth. For instance, when targeting fully faceted nanocrystals with their lowest-energy absorption peak at ~580 nm (Abs-580, ~4.2 nm in size), the absorption peak of the seeds should be below ~530 nm (~2.7 nm in size) (Figure S3, Supporting Information). This seemed to be reasonable, given the seeds being spherical nanocrystals, and thus, completion of

DOI: 10.1021/jacs.6b00674
J. Am. Chem. Soc. 2016, 138, 6475−6483

the targeted layer-by-layer growth to yield a fully faceted structure would require significant volume increase.

Characterization of Faceted Nanocrystals. All CdSe magic-size clusters reported in literature were regular tetrahedrons,[9,10,12,15,18,24] whose two-dimensional projection should be equilateral triangle and monodisperse. The resulting nanocrystals of Step 1 (Figure 1b) appeared to be regularly faceted under TEM, but their two-dimensional projections were neither equilateral nor monodisperse (Figures 1b and 2c–e). However, their absorption and PL spectra were extremely sharp (Figures 2f and 3a), and their photoluminescence excitation

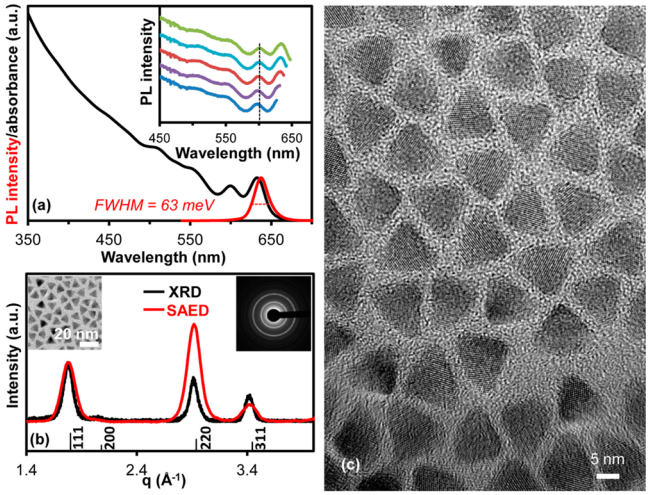

Figure 3. (a) Typical UV–vis and PL spectra of fully faceted nanocrystals. Inset: PLE spectra with emission at 628, 632, 638, 642, and 648 nm, respectively. (b) XRD pattern and integrated intensity profile from SAED pattern of fully faceted nanocrystals. Inset: The TEM image (left) and SAED pattern (right) of the sample. (c) HRTEM image of the same sample in (b). All spectra were intensity-normalized for comparison.

(PLE) spectra at different emission positions nearly overlapped with each other (see Figure 3a as example). A possible explanation for the inconsistency between the TEM appearance and optical properties would be that the shape of monodisperse and fully faceted nanocrystals was a low-symmetry polyhedron, which would result in different types of two-dimensional projections.

Figure 3b shows that the X-ray powder diffraction (XRD) pattern was in accordance with the standard pattern. Conversely, the Selected-Area Electron Diffraction (SAED) pattern possessed an excessively strong (220) peak, indicating preferential orientation of the nanocrystals, i.e., with their ⟨110⟩ zone axis perpendicular to TEM substrates. Evidently, such preferential orientation would be difficult for those CdSe magic-size clusters reported in literature, tetrahedrons with four equal (111) facets.[9,10,12,15,18,24]

Under high-resolution TEM (HRTEM) (Figure 3c), three types of two-dimensional lattice patterns constituted >90% of the nanocrystals. Nanocrystals with ⟨100⟩ zone axis perpendicular to the TEM substrate were ~5%, which appeared as isosceles triangles with their top angle as right angle. The basal side of these right-angle triangles were of low contrast and not well-defined (see Figure 4a for high-magnification image). Consistent with SAED (Figure 3b), majority of the nanocrystals pointed their ⟨110⟩ zone axis perpendicular to the TEM substrate, which appeared as isosceles triangles with defined

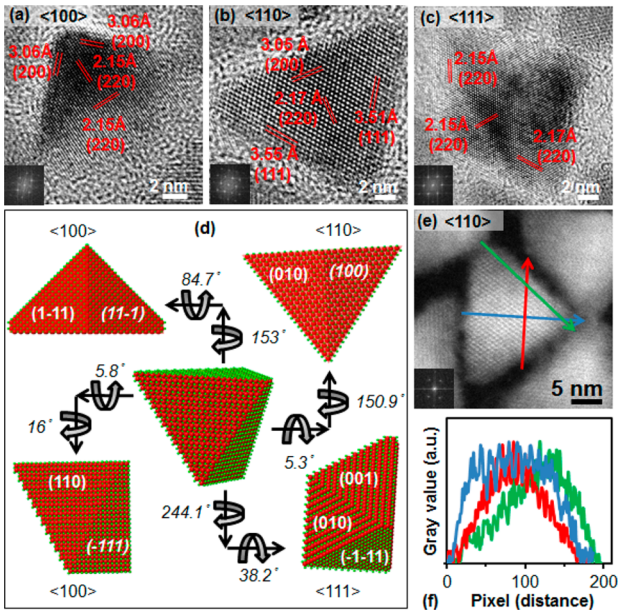

Figure 4. (a–c) HRTEM images of three types of two-dimensional projections of hexahedral nanocrystals. Inset: fast Fourier transform (FFT) patterns. (d) Relationship between the hexahedral shape and three types of two-dimensional projections (green, Cd; red, Se). (e) Lattice-resolved HAADF-STEM image of the hexahedra and (f) contrast profiles along three directions labeled in (e).

edges (see Figure 4b for a high-magnification image).The third type (see Figure 4c for high-magnification image) of orientation, with the ⟨111⟩ zone axis perpendicular to the substrate, was in a low population (<1%), whose population increased slightly as the fully faceted nanocrystals grew in dimensions. The third type appeared as quadrilateral (Figure 4c).

Figure 4d illustrates that all three types of two-dimensional projections, including two subtypes for the ⟨100⟩ projection, were related to a low-symmetry (C_s group with single mirror plane perpendicular to the (110) facet) hexahedron terminated with three (100) facets, two (111) facets, and one (110) facet. Given the low-contrast nature at the base of either of two subtypes of the ⟨100⟩ projection, it would be difficult to distinguish them from each other by high-resolution TEM. Confirmation of this structure was further provided by Lattice-resolved High Angle Annular Dark Filed Scanning Transmission Electron Microscopy (HAADF-STEM). Figure 4e shows the lattice-resolved image of one hexahedral nanocrystal with its ⟨110⟩ zone axis perpendicular to the substrate. For this type of lattice-resolved image, the main type of orientation as mentioned above, contrast along three representative directions (Figure 4e,f) was found in excellent agreement with the hexahedral model of the faceted nanocrystals.

All these results revealed that the faceted nanocrystals were qualitatively different in surface termination and shape from those of the CdSe magic-size clusters reported in literature. For each individual facet on the hexahedron, the (110) facet was much larger than either (100) facet, and either of the (111) facets was the smallest among the six facets. The total area ratio of three types of low-index facets was, respectively, 49%, 23%, and 28% for (100), (110), and (111) facets. The (100) and (111) facets are polar ones and can be fully coordinated with carboxylate ligands.[39,43–47] Conversely, the (110) facet should be terminated with both Cd and Se ions if no surface

DOI: 10.1021/jacs.6b00674
J. Am. Chem. Soc. 2016, 138, 6475–6483

reconstruction involved. Though polar facets were identified exclusively in some reports,[43−45,47−50] observation of nonpolar facets was not rare.[48−53] As an extreme example, wurtzite CdSe nanobelts and nanorods were formed with polar (001) facets as two small tips and their large sides were typically terminated with nonpolar facets.[54−57]

Conversion from Hexahedral Nanocrystals to Spherical Ones. For two CdSe nanocrystals with the same volume, the specific surface area per particle of the low-symmetry hexahedral nanocrystal (Figure 4) is ∼31% higher on average than that of the corresponding spherical one (Table 1). Thus, hexahedral nanocrystals should be thermodynamically less stable than the other, though they are kinetically easy to form under the layer-by-layer growth mode. It is interesting to note that the specific surface area of regular tetrahedrons is further larger than that of the corresponding low-symmetry hexahedra, i.e., ∼50% increase from that of spheres. In the tiny size regime, interior atoms are very limited and optimization of surface configuration becomes the dominating factor, which results in stable magic-size clusters in that special size regime.

Table 1. Comparison of Hexahedral and Corresponding Spherical Nanocrystals after Conversion[a]

volume (nm^3)	shape	UV−vis (nm)	PL (nm)	fwhm (meV)	altitude/size (nm)	specific surface area (nm^{-1})
77.5	hexahedral	620	626	70.5	5.6	1.48
	spherical	625	631	68.5	5.5 *(5.3)*	1.13
117.1	hexahedral	632	638	62.9	6.5	1.29
	spherical	638	643	61.6	6.2 *(6.1)*	0.99
174.7	hexahedral	652	657	61.0	7.5	1.13
	spherical	658	662	61.8	7.1 *(6.9)*	0.87
240.3	hexahedral	668	671	57.4	8.4	1.02
	spherical	672	676	58.5	7.9 *(7.7)*	0.78
416.7	hexahedral	685	689	55.7	10.2	0.85
	spherical	690	694	56.9	9.4 *(9.3)*	0.65
930.4	hexahedral	705	708	55.8	13.5	0.65
	spherical	710	713	58.0	12.4 *(12.1)*	0.50

[a]The altitude of the hexahedra refers to the altitude of the (110) isosceles triangle. Numbers in parentheses are the theoretical sizes of spheres.

The low-symmetry hexahedral nanocrystals were found to be stable under the growth conditions as mentioned above. After removal of the excess cadmium alkanoates in the solution by purification (Figure S5, Supporting Information), conversion to spherical ones was accelerated substantially. Purified hexahedra were converted nicely to spherical ones with narrow size distribution (Figures 5a,b), though the temperature was the same as the formation temperature of the hexahedral nanocrystals. These results were in good accordance with the original design, that layer-by-layer growth for formation of the fully faceted nanocrystals could only be enabled by offering a sufficient ligand coverage on nanocrystals. The spherical nanocrystals in Figure 5b appeared to be monodisperse, i.e., with relative standard deviation (Rsd) being 3−5% calculated with ∼600 nanocrystals. By assuming the volume as constant, the average size (diameter) of the spherical nanocrystals was found to be in agreement with the dimension of the corresponding hexahedra (Table 1). All these supported the conversion was through intraparticle ripening.

Both XRD and SAED patterns of the spherical nanocrystals obtained by the conversion resembled a standard one of zinc blende CdSe nanocrystals (Figure 5c), which was in stark contrast with those of the low-symmetry hexahedra (Figure 3b). Simultaneously, lattice fringes of spherical nanocrystals under HRTEM (Figures 5c (inset) and S6, Supporting Information) were no longer dominated by the ones with the ⟨110⟩ zone axis perpendicular to TEM substrates.

The conversion shifted the UV−vis and PL spectra of the nanocrystals to the low-energy direction slightly (Figure 5d),

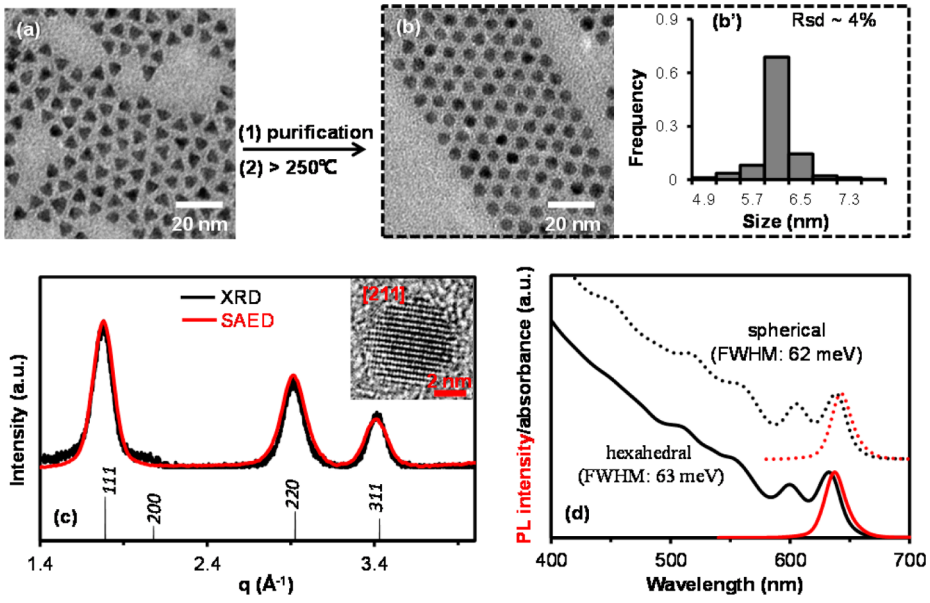

Figure 5. TEM images of (a) before and (b) after the conversion of the hexahedral nanocrystals. (b′) Size distribution histogram of the resulting spherical nanocrystals. (c) XRD pattern and integrated intensity profile from SAED pattern of the spherical nanocrystals. Inset: HRTEM image of one type of two-dimensional projections for spherical nanocrystals. (d) Normalized UV−vis absorption and PL emission of CdSe nanocrystals before (solid line) and after (dashed line) the conversion.

DOI: 10.1021/jacs.6b00674
J. Am. Chem. Soc. 2016, 138, 6475−6483

which should be related to the somewhat reduced quantum confinement of the resulting spherical dots. However, sharpness of UV−vis absorption peaks and the PL fwhm remained the same (Figure 5d and Table 1). Temporal evolution of optical properties of nanocrystals during the conversion was closely followed (Figure S7, Supporting Information). The spectra evolved from that of the hexahedral nanocrystals to corresponding spherical ones monotonically without abrupt change. Under the reaction conditions for the conversion in Figure 5, prolonged heating (up to ∼4 h) after conversion did not vary either UV or PL spectra. These results suggested that the conversion was intraparticle ripening and no involvement of interparticle ripening—classic Ostwald ripening. To further confirm this, conversion reaction was performed with a mixture of purified hexahedral nanocrystals with two distinguishable sizes under TEM and optical spectra. Figure 6a,b illustrates the

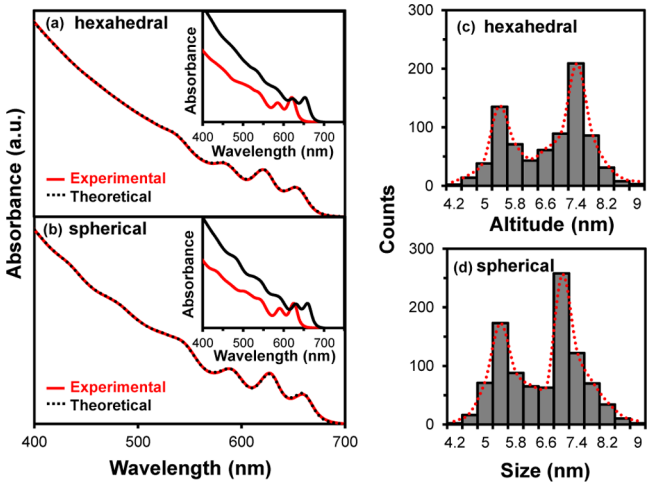

Figure 6. (a) Before and (b) after the conversion reaction, UV−vis absorption spectra of experimental (solid line) and superposition (dashed line) for a mixture composed of two sizes of nanocrystals. The superposition was obtained using the spectra of the corresponding pure samples (inset). (a) Before and (b) after the conversion reaction, size distribution histograms.

experimental and superposition absorption spectra of one set of such a mixture before and after the conversion, with the spectra of two pure samples shown in the inset. Excellent consistency between the experimental and theoretical results of the absorption (Figure 6b) and PL measurements (Figure S8, Supporting Information) strongly suggested that two sizes were independent from each other during the conversion. Figure 6c,d further shows that conversion did not affect the size distribution of the mixture. These results were considered as strong evidence of nonexistence of interparticle ripening in the conversion outlined in Figure 5.

Temperature-Dependent Conversion from Hexahedral to Spherical Nanocrystals. The conversion process was followed quantitatively by taking aliquots at given time intervals for TEM measurements to analyze the shape population (see Experimental Section for detail). For convenience, all results in Figure 7 were labeled with the corresponding lowest-energy UV−vis peak of the initial hexahedra. Results clearly revealed that the conversion was accelerated greatly by increasing temperature and suppressed by increasing the size. Because of its apparent dependence on the ligand concentration discussed above, it would be reasonable to assume origin of the temperature dependence in Figure 7 was due to a significant activation energy of desorption of the ligands. If this was true, the activation energy should be on the order of the bonding energy of RCOO-Cd bond, i.e., ∼17 kJ/mol.[58]

The population decay of a given size of the hexahedral nanocrystals at a given temperature followed a single-exponential kinetics, indicating a first-order reaction as expected for intraparticle ripening. Those exponential fittings in Figure 7a−e yielded the rate constant (k) for each first-order kinetics. For a given size, we plotted k versus inverse of absolute temperature (T) and obtained a good linear fit (Figure 7f). For Arrehnius-type kinetics, $k = A\ e^{-(Ea/RT)}$. Here E_a and A are activation energy and pre-exponential factor, respectively. R is the gas constant. A universal activation energy (E_a) was obtained from Figure 7f regardless of the size of the hexahedra, i.e., 160 ± 5 kJ/mol for all cases. This value was about 1 order of magnitude larger than that expected for ligand dynamics. The bonding energy in CdSe bulk crystal is about 310 kJ/mol.[59] Thus, the experimental activation energy suggested that the rate-limiting step for the conversion was likely the atom motion on the surface of nanocrystals.

The universal activation energy implied strong size-dependence of the pre-exponential factor (Figure S9, Supporting Information). Though current work could not offer a clear picture of A, it should include a few contributions. The first contribution should be the size-dependent surface area. The larger the surface area of the hexahedra is, the slower the population decay would be. The second one should be the ligand dynamics, which would be the prerequisite for the rate-limiting step to occur. Evidently, the number of ligands on a hexahedron should be strongly dependent on the size of the nanocrystals. To support the latter hypothesis, further experimental results (Figure S10, Supporting Information) confirmed that variation of types of carboxylate ligands did not change the activation energy but the pre-exponential factor.

Furthermore, concentration of the hexahedral nanocrystals in a reaction solution did not affect the kinetics of the conversion (Figure S11, Supporting Information). This was in stark contrast to the strong influence of concentration of the ligands as described above but expected for intraparticle ripening.

Promotion of Conversion of the Hexahedral to Spherical Nanocrystals by Fatty Amines. Results in Figure 7 indicate that, even after removal of extra cadmium alkanote ligands in the solution, the conversion of the hexahedral nanocrystals was very slow for very large ones (see one example in Figure 7e). By addition of oleylamine into the reaction solution, conversion of the large hexahedra could readily occur at 250 °C with unity yield and narrow size distribution (Figure 8a,b,b′). In fact, very large hexahedra with their lowest-energy absorption peak at ∼705 nm, approaching the band gap of CdSe bulk crystals, could complete the conversion to yield monodisperse spherical nanocrystals with ∼12.4 nm in size (Figure S12, Supporting Information). The ensemble PL fwhm of the spherical nanocrystals obtained with amine ligands remained as narrow as the corresponding hexahedral nanocrystals (Figure 8c).

Conversion kinetics of the hexahedra with addition of fatty amines was studied (Figures 8d and S13), which quantitatively confirmed the drastic acceleration of amines. Consistent with the conclusion in the above subsection, the activation energy, corresponding to the slope of the linear plots in Figure 8d, was not affected by addition of fatty amines but the pre-exponential factor increased substantially (Figure 8d).

DOI: 10.1021/jacs.6b00674
J. Am. Chem. Soc. 2016, 138, 6475−6483

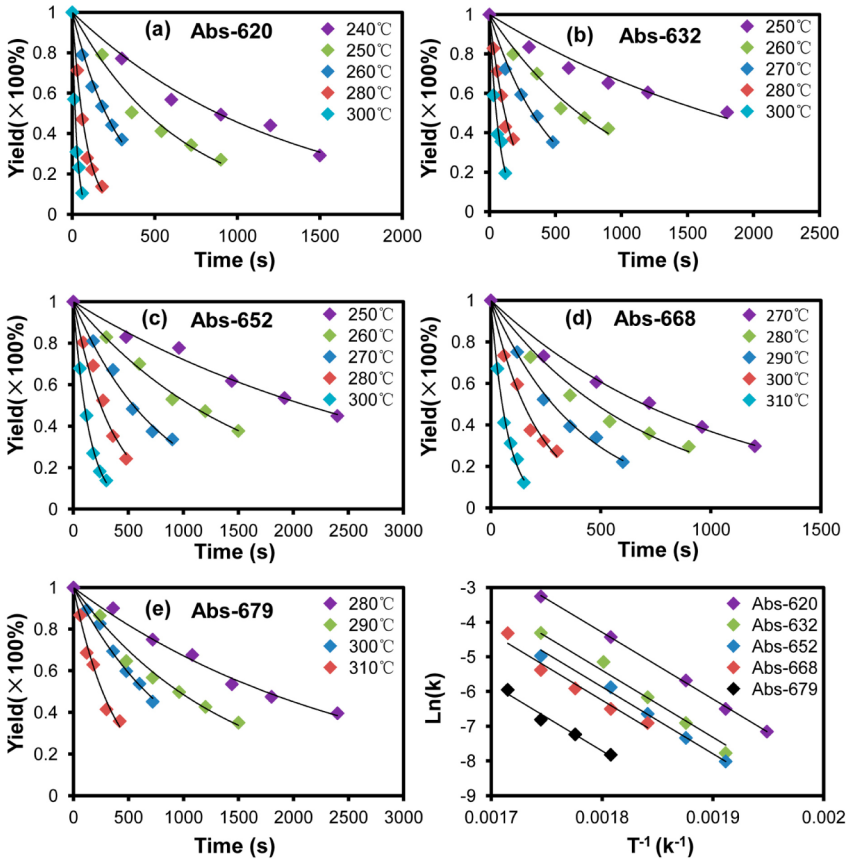

Figure 7. (a–e) Temporal evolution of population of the hexahedra with different sizes during the conversion at varies temperatures. The solid lines are single-exponential fitting. (f) Arrhenius plots for the conversion of the hexahedra.

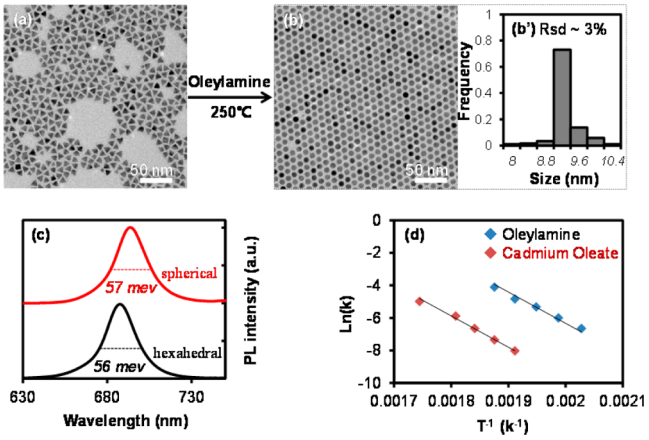

Figure 8. TEM images of CdSe nanocrystals before (a) and after (b) the conversion of the hexahedra with addition of fatty amines. (b′) Size distribution histogram of the resulting spherical nanocrystals. (c) PL spectra of CdSe nanocrystals before (black line) and after (red line) the conversion with fatty amines. (d) Arrhenius plots of the conversion of the hexahedral nanocrystals with (blue diamonds) and without (red diamonds) addition of oleylamine.

It should be noted that addition of amines also accelerated interparticle ripening, namely the regular Ostwald ripening.[26] At 250 °C with addition of fatty amines, conversion of the hexahedral nanocrystals occurred quite rapidly to yield spherical nanocrystals with nearly monodisperse size distribution (Figure 8). If the reaction proceeded further after completion of the conversion, the size distribution would start to worsen and the ensemble PL fwhm would increase noticeably (Figure S14, Supporting Information).

Fatty amines have been widely applied for synthesis of high quality nanocrystals in nonaqueous solutions.[26] Results in Figure 8 suggest that promotion of surface ligand dynamics could be one of the benefits. Active ligand dynamics not only enables growth of nanocrystals but also promotes intraparticle ripening to reach a uniform shape (spherical) for all nanocrystals. However, if targeting nonspherical shapes, amine ligands should be avoided.

Comparison of Single-Dot PL and Ensemble PL. When the last dose of the Se-Sus was replaced by a S solution in ODE (see detail in the Experimental Section), the resulting nanocrystals would be CdSe/CdS core/shell nanocrystals. These core/shell nanocrystals, approximately with ∼2 monolayers of CdS shell, were found to be sufficiently stable for recording single-dot PL spectrum using a standard setup.[60] Detailed study of these interesting core/shell nanocrystals shall be published separately, and here we shall apply them for comparison of single-dot and ensemble PL properties.

Figure 9a shows a representative PL spectrum of a single dot along with the corresponding ensemble PL spectrum. Both peak width and contour of two spectra resembled each other. Figure 9b summaries the single-dot PL fwhm for multiple core/shell nanocrystals, which fluctuated around the ensemble value (the red line). Inspection of temporal evolution of the single-dot PL spectrum revealed that the PL fwhm in Figure 9b might include a certain degree of spectral drifting (Figure 9c) that was reported previously.[61]

DOI: 10.1021/jacs.6b00674
J. Am. Chem. Soc. 2016, 138, 6475–6483

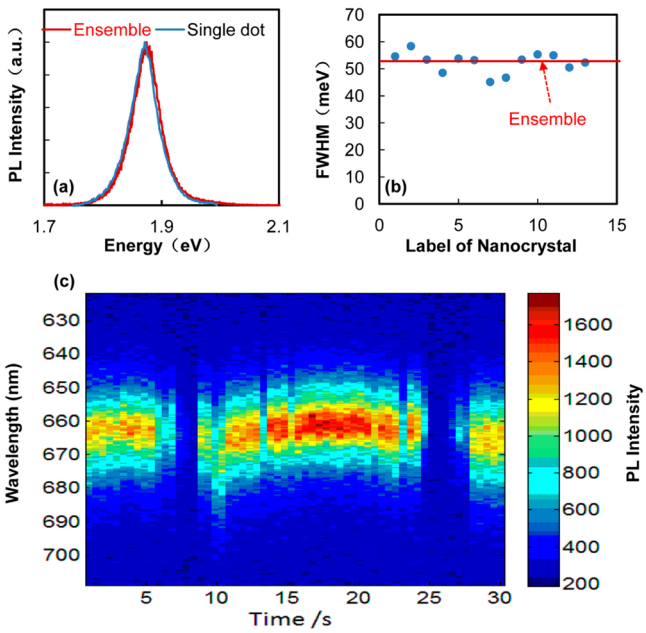

Figure 9. (a) PL spectra obtained with ensemble measurements for the CdSe/CdS core/shell hexahedra in solution and a single-dot on a glass slide. (b) Distribution of PL fwhm of multiple core/shell nanocrystals with the ensemble value as reference. (c) Temporal evolution of the PL of one CdSe/CdS core/shell nanocrystal under continuous excitation (bin time being 1 s).

CONCLUSION

In summary, by varying the surface ligand dynamics, growth of colloidal nanocrystals could be reproducibly controlled in different modes, i.e., layer-by-layer growth, intraparticle ripening, and interparticle ripening. With excessively high concentrations of cadmium alkanotes as ligands, layer-by-layer growth resulted in CdSe hexahedral nanocrystals with six low-index facets, which offered a unique tool to control the final volume of the nanocrystals. Decrease of ligand passivation and/or increase of reaction temperature could activate intraparticle ripening of the hexahedral nanocrystals, given their significantly larger specific surface area than that of spherical ones. In comparison, classic Ostwald ripening (interparticle ripening) was found to require the lowest ligand passivation. Layer-by-layer growth plays a dominating role on growth of bulk crystals, in which specific surface area is not a sensitive measure and growth of crystals could be approximated as local/surface events. Specific surface area is significant and size dependent in nanometer size regime, which enables interplay between layer-by-layer growth and intraparticle ripening. These understandings not only reveal new insights on crystal growth in nanometer size regime but also promote development of synthetic chemistry of nanocrystals with not easily accessible properties.

EXPERIMENTAL SECTION

Chemicals. Cadmium oxide (CdO, 99.998%), myristic acid (98%), stearic acid (90+%), selenium power (200 mesh, 99.999%), 1-octadecene (ODE, 90%), tetramethylammonium hydroxide (98%), and oleic acid (99% or 90%) were purchased from Alfa-Aesar. Cadmium acetate dihydrate ($Cd(Ac)_2 \cdot 2H_2O$, AR) was purchased from Aladdin Reagents. Oleylamine (98+%) was purchased from Aldrich. All organic solvents were obtained from Sinopharm Reagents. All chemicals were used directly without any further purification.

Synthesis of Cd Myristate. Cd acetate (10 mmol) was dissolved in methanol (20 mL) in a 50 mL flask. In another flask (500 mL), myristic acid (20 mmol) and tetramethylammonium hydroxide (20 mmol) were dissolved in100 mL of methanol by stirring for 20 min. To this solution was added the Cd acetate solution dropwise with vigorous stirring. White precipitation indicated formation of Cd myristate and stirring was continued for another 20 min after completion of addition of the Cd acetate solution. The precipitate was separated and washed three times with methanol by filtration. The final precipitate was dried under vacuum at room temperature overnight before using.

Synthesis of CdSe Hexahedral Nanocrystals. The Se-suspension (Se-Sus) was prepared by dispersing Se powder (0.0120 g, 0.05 mmol) in ODE (3 mL) by sonication for 5 min for synthesis of the dot-shaped nanocrystals as seeds. In a typical synthesis of the seeds, CdO (0.1280 g, 1 mmol) and myristic acid (0.5 g, 2.2 mmol) were loaded into a 25 mL three-neck flask with 4 mL of ODE. After stirring and argon bubbling for 10 min, the mixture was heated to 290 °C to obtain a colorless solution. The temperature was reduced to 250 °C, and 1 mL of the Se-Sus was injected swiftly into the hot solution, which brought down the temperature to 220 °C. The reaction temperature was kept at 250 °C for ~10 min for further growth to yield CdSe nanocrystal seeds. For seeds with the lowest absorption peak beyond ~600 nm, they were produced by the conversion of the hexahedral nanocrystals after purification (see detail below).

For growth of the hexahedral nanocrystals with the seeds described above, another Se-suspension was prepared by mixing 0.0240 g of selenium powder in 3 mL of ODE (0.1 mmol/mL). The growth temperature was set at 250 °C. Prior to growth of the hexahedral nanocrystals, ~1.5 mmol oleic acid was dropwise added into the reaction flask at 12 mL/h and followed by stirring for another 5 min. Consequently, one dose of the Se-Sus (0.1 mL) was loaded into a syringe and dropwise added into the reaction flask at 0.9 mL/h. After one dose of the Se-Sus was added, the reaction solution was allowed to react for 10 min under the given conditions. This reaction cycle, addition of one dose of Se-Sus and reaction for 10 min, was continued until a targeted size of CdSe hexahedral nanocrystals was obtained.

Aliquots (~0.05 mL) were taken for UV−vis, PL, and TEM measurements to monitor the reaction. When the desired size of CdSe hexahedra was reached, the reaction mixture was annealed for another 15 min before cooling down to room temperature in air. Synthesis of the hexahedral nanocrystals with different fatty acid and/or fatty acid salts were carried out using the same procedure.

The above procedure was varied slightly for growth of the hexahedral nanocrystals with small dimensions. Synthesis of the seeds with the lowest absorption peak below ~550 nm followed a procedure in literature[38] with a low concentration of cadmium fatty acid salt (~0.2 mmol). For the related growth of the hexahedral nanocrystals, variations from the procedure described above were made to accommodate the low stability of small nanocrystals. Specifically, growth temperature was ~210 °C and oleic acid was replaced by 0.2 mmol of myristic acid.

Isolation/Purification of the Hexahedral Nanocrystals. Typically, the reaction mixture with the hexahedra (1−1.5 mL) was loaded into a 4 mL vial and kept at 50 °C as a clear solution. Into the vial, a mixture of acetone, chloroform, and methanol (volume ratio 1:1:1, 2−3 mL in total) was added. The vial was placed in a centrifugation at ~50 °C and centrifuged for ~20 s. The supernatant was removed quickly. The nanocrystals precipitate was dissolved in ~0.5 mL toluene, and into it, the mixture of acetone, chloroform, and methanol was added again to start another cycle of precipitation, centrifugation, decantation, and dissolution. This purification procedure was repeated twice. The last step of purification was performed by precipitation from toluene solution using acetone only at room temperature. For the conversion reactions, these final products were dissolved in a given volume of ODE.

Conversion of the Hexahedral Nanocrystals into Spherical Ones. Three different approaches were developed to convert the hexahedral nanocrystals into spherical ones. The small ones (with the lowest UV−vis absorption peak below 640 nm) could be directly

DOI: 10.1021/jacs.6b00674
J. Am. Chem. Soc. 2016, 138, 6475−6483

converted by simply increasing temperature of the reaction mixture up to ~300−310 °C for ~30 min. The conversion process was followed by UV−vis, PL, and TEM measurements. After the conversion, the reaction mixture was allowed to cool to room temperature in air to stop the reaction. For the second approach, the purified hexahedra dissolved in 0.5 mL of ODE were injected into 5 mL of ODE at 240−310 °C under Ar flow. The reaction time depended on the size of the hexahedral nanocrystals, the conversion temperature, and the purpose of the experiments. Needle-tip aliquots were taken at given intervals for UV−vis, PL, and TEM measurements. For the third approach, the ODE in the flask was replaced by 1:1 mixture of ODE and oleylamine, and the reaction temperature was in the range between 220 and 300 °C depended on the size of the hexahedral nanocrystals and the purpose of the experiments.

For the conversion of mixed hexahedra with two different sizes, two types of purified hexahedra were mixed together with a known proportion and injected into preheated ODE. Simultaneously, each type of the hexahedral nanocrystals underwent the same conversion reaction as the references.

Kinetics of the Conversion. The conversion reactions were performed using the procedures described above. The population of the hexahedral nanocrystals for an aliquots was obtained by examining ~1000 particles in a TEM image. For a given reaction, all population values for kinetic analysis were normalized by the initial value. For any individual nanocrystal, it was classified into two categories, either hexahedra or converted. The criterion for the classification was the angles of a given two-dimensional projection. As a great majority of the hexahedral nanocrystals preferentially oriented with their ⟨110⟩ zone axis perpendicular to TEM substrates, an individual nanoparticle would be examined against the standard appearance of an equal-lateral triangle mainly using the two bottom angles. If a nanocrystal was found to not be related to the ones with ⟨110⟩ zone axis perpendicular to the substrate, it would then be compared with a two-dimensional projection with a right triangle, which was the common feature for the other two types of orientations of the hexahedral nanocrystals.

Synthesis of CdSe/CdS Core/Shell Hexahedral Nanocrystals. In a typical synthesis, the purified hexahedral core nanocrystals (lowest-energy absorption peak at 632 nm) in ODE and about 0.8 mmol cadmium myristate were loaded into 5 mL of ODE. After stirring and argon bubbling for 10 min, the mixture was heated to 250 °C and 1.5 mL of oleic acid was dropwise added. Subsequently, an S solution in ODE (0.1 mmol/mL) was dropped in dose (0.1 mL per dose) by a syringe. The reaction time after each dose was ~10 min. Needle-tip aliquots were taken and dissolved in toluene for UV−vis and PL measurements to monitor the reaction. When the desired shell thickness was reached, the reaction was stopped by allowing the reaction mixture to cool down in air.

Measurements and Characterization. UV−vis spectra were taken on an Analytik Jena S600 UV−visible spectrophotometer. PL spectra were recorded by an Edinburgh Instruments FLS920 spectrometer. XRD measurements were carried out on a Rigaku Ultimate-IV X-ray diffractometer operated at 40 kV/30 mA with Cu Kα line (λ = 1.5418 Å). TEM images and SAED patterns were taken on a Hitachi 7700 transmission electron microscope at 100 kV, and the nanocrystals were deposited onto an ultrathin carbon film on a copper grid. HRTEM images were taken on a JEM 2100F transmission electron microscope at 300 kV. Lattice-resolved HAADF-STEM analysis was performed on a spherical aberration corrected FEI Titan G^2 80−200 STEM with ChemiSTEM technology at 200 kV.

■ ASSOCIATED CONTENT

Supporting Information

The Supporting Information is available free of charge on the ACS Publications website at DOI: 10.1021/jacs.6b00674.

Additional experimental data (PDF)

■ AUTHOR INFORMATION

Corresponding Author

*xpeng@zju.edu.cn

Notes

The authors declare no competing financial interest.

■ ACKNOWLEDGMENTS

This work was supported by the National Natural Science Foundation of China (Grants 21233005 and 91433204) and Fundamental Research Fund for the Central Universities (Grant 2014FZA3006).

■ REFERENCES

(1) Brus, L. E. *J. Chem. Phys.* **1984**, *80*, 4403.
(2) Colvin, V. L.; Schlamp, M. C.; Alivisatos, A. P. *Nature* **1994**, *370*, 354.
(3) Coe, S.; Woo, W. K.; Bawendi, M.; Bulovic, V. *Nature* **2002**, *420*, 800.
(4) Dai, X. L.; Zhang, Z. X.; Jin, Y. Z.; Niu, Y.; Cao, H. J.; Liang, X. Y.; Chen, L. W.; Wang, J. P.; Peng, X. G. *Nature* **2014**, *515*, 96.
(5) Bruchez, M., Jr,.; Moronne, M.; Gin, P.; Weiss, S.; Alivisatos, A. P. *Science* **1998**, *281*, 2013.
(6) Chan, W. C. W.; Nie, S. M. *Science* **1998**, *281*, 2016.
(7) Klimov, V. I.; Mikhailovsky, A. A.; Xu, S.; Malko, A.; Hollingsworth, J. A.; Leatherdale, C. A.; Eisler, H. J.; Bawendi, M. G. *Science* **2000**, *290*, 314.
(8) Michler, P.; Kiraz, A.; Becher, C.; Schoenfeld, W. V.; Petroff, P. M.; Zhang, L. D.; Hu, E.; Imamoglu, A. *Science* **2000**, *290*, 2282.
(9) Herron, N.; Calabrese, J. C.; Farneth, W. E.; Wang, Y. *Science* **1993**, *259*, 1426.
(10) Vossmeyer, T.; Reck, G.; Katsikas, L.; Haupt, E. T. K.; Schulz, B.; Weller, H. *Science* **1995**, *267*, 1476.
(11) Soloviev, V. N.; Eichhofer, A.; Fenske, D.; Banin, U. *J. Am. Chem. Soc.* **2000**, *122*, 2673.
(12) Soloviev, N. V.; Eichhofer, A.; Fenske, D.; Banin, U. *J. Am. Chem. Soc.* **2001**, *123*, 2354.
(13) Kasuya, A.; Sivamohan, R.; Barnakov, Y. A.; Dmitruk, I. M.; Nirasawa, T.; Romanyuk, V. R.; Kumar, V.; Mamykin, S. V.; Tohji, K.; Jeyadevan, B.; Shinoda, K.; Kudo, T.; Terasaki, O.; Liu, Z.; Belosludov, R. V.; Sundararajan, V.; Kawazoe, Y. *Nat. Mater.* **2004**, *3*, 99.
(14) Bowers, M. J.; McBride, J. R.; Rosenthal, S. J. *J. Am. Chem. Soc.* **2005**, *127*, 15378.
(15) Zheng, N. F.; Bu, X. H.; Lu, H. W.; Zhang, Q. C.; Feng, P. Y. *J. Am. Chem. Soc.* **2005**, *127*, 11963.
(16) Jose, R.; Zhanpeisov, N. U.; Fukumura, H.; Baba, Y.; Ishikawa, M. *J. Am. Chem. Soc.* **2006**, *128*, 629.
(17) Kudera, S.; Zanella, M.; Giannini, C.; Rizzo, A.; Li, Y. Q.; Gigli, G.; Cingolani, R.; Ciccarella, G.; Spahl, W.; Parak, W. J.; Manna, L. *Adv. Mater.* **2007**, *19*, 548.
(18) Corrigan, J. F.; Fuhr, O.; Fenske, D. *Adv. Mater.* **2009**, *21*, 1867.
(19) Dukes, A. D.; McBride, J. R.; Rosenthal, S. J. *Chem. Mater.* **2010**, *22*, 6402.
(20) Cossairt, B. M.; Owen, J. S. *Chem. Mater.* **2011**, *23*, 3114.
(21) Yu, K. *Adv. Mater.* **2012**, *24*, 1123.
(22) Newton, J. C.; Ramasamy, K.; Mandal, M.; Joshi, G. K.; Kumbhar, A.; Sardar, R. *J. Phys. Chem. C* **2012**, *116*, 4380.
(23) Harrell, S. M.; McBride, J. R.; Rosenthal, S. J. *Chem. Mater.* **2013**, *25*, 1199.
(24) Beecher, A. N.; Yang, X. H.; Palmer, J. H.; LaGrassa, A. L.; Juhas, P.; Billinge, S. J. L.; Owen, J. S. *J. Am. Chem. Soc.* **2014**, *136*, 10645.
(25) Murray, C. B.; Kagan, C. R.; Bawendi, M. G. *Annu. Rev. Mater. Sci.* **2000**, *30*, 545.
(26) Peng, X. G. *Nano Res.* **2009**, *2*, 425.
(27) Cui, J.; Beyler, A. P.; Coropceanu, I.; Cleary, L.; Avila, T. R.; Cordero, J. M.; Heathcote, S. L.; Harris, D. K.; Chen, O.; Cao, J. S.; Bawendi, M. G. *Nano Lett.* **2016**, *16*, 289.

DOI: 10.1021/jacs.6b00674
J. Am. Chem. Soc. 2016, 138, 6475−6483

(28) Qu, L. H.; Peng, X. G. *J. Am. Chem. Soc.* **2002**, *124*, 2049.
(29) Peng, X. G.; Wickham, J.; Alivisatos, A. P. *J. Am. Chem. Soc.* **1998**, *120*, 5343.
(30) Thessing, J.; Qian, J. H.; Chen, H. Y.; Pradhan, N.; Peng, X. G. *J. Am. Chem. Soc.* **2007**, *129*, 2736.
(31) Chen, Y. F.; Johnson, E.; Peng, X. G. *J. Am. Chem. Soc.* **2007**, *129*, 10937.
(32) Rempel, J. Y.; Bawendi, M. G.; Jensen, K. F. *J. Am. Chem. Soc.* **2009**, *131*, 4479.
(33) Cho, K. S.; Talapin, D. V.; Gaschler, W.; Murray, C. B. *J. Am. Chem. Soc.* **2005**, *127*, 7140.
(34) Ji, X. H.; Song, X. N.; Li, J.; Bai, Y. B.; Yang, W. S.; Peng, X. G. *J. Am. Chem. Soc.* **2007**, *129*, 13939.
(35) Peng, Z. A.; Peng, X. G. *J. Am. Chem. Soc.* **2001**, *123*, 1389.
(36) Alivisatos, A. P. *Science* **1996**, *271*, 933.
(37) Mullin, J. W. *Crystallization*; 3rd ed.; Butterworth: Oxford, 1997.
(38) Pu, C. D.; Zhou, J. H.; Lai, R. C.; Niu, Y.; Nan, W. N.; Peng, X. G. *Nano Res.* **2013**, *6*, 652.
(39) Voznyy, O. *J. Phys. Chem. C* **2011**, *115*, 15927.
(40) Pradhan, N.; Reifsnyder, D.; Xie, R. G.; Aldana, J.; Peng, X. G. *J. Am. Chem. Soc.* **2007**, *129*, 9500.
(41) Chen, O.; Yang, Y. A.; Wang, T.; Wu, H. M.; Niu, C. G.; Yang, J. H.; Cao, Y. C. *J. Am. Chem. Soc.* **2011**, *133*, 17504.
(42) Ji, X. H.; Copenhaver, D.; Sichmeller, C.; Peng, X. G. *J. Am. Chem. Soc.* **2008**, *130*, 5726.
(43) Liu, L. P.; Zhuang, Z. B.; Xie, T.; Wang, Y. G.; Li, J.; Peng, Q.; Li, Y. D. *J. Am. Chem. Soc.* **2009**, *131*, 16423.
(44) Li, Z.; Peng, X. G. *J. Am. Chem. Soc.* **2011**, *133*, 6578.
(45) Saruyama, M.; So, Y. G.; Kimoto, K.; Taguchi, S.; Kanemitsu, Y.; Teranishi, T. *J. Am. Chem. Soc.* **2011**, *133*, 17598.
(46) Debnath, S.; Cherian, R.; Mahadevan, P. *J. Phys. Chem. C* **2013**, *117*, 21981.
(47) Boles, M. A.; Talapin, D. V. *J. Am. Chem. Soc.* **2014**, *136*, 5868.
(48) Fang, C. M.; van Huis, M. A.; Vanmaekelbergh, D.; Zandbergen, H. W. *ACS Nano* **2010**, *4*, 211.
(49) Choi, J. J.; Bealing, C. R.; Bian, K. F.; Hughes, K. J.; Zhang, W. Y.; Smilgies, D. M.; Hennig, R. G.; Engstrom, J. R.; Hanrath, T. *J. Am. Chem. Soc.* **2011**, *133*, 3131.
(50) Bealing, C. R.; Baumgardner, W. J.; Choi, J. J.; Hanrath, T.; Hennig, R. G. *ACS Nano* **2012**, *6*, 2118.
(51) Mahler, B.; Lequeux, N.; Dubertret, B. *J. Am. Chem. Soc.* **2010**, *132*, 953.
(52) Bose, R.; Manna, G.; Pradhan, N. *J. Phys. Chem. C* **2013**, *117*, 18762.
(53) Knittel, F.; Gravel, E.; Cassette, E.; Pons, T.; Pillon, F.; Dubertret, B.; Doris, E. *Nano Lett.* **2013**, *13*, 5075.
(54) Pradhan, N.; Xu, H. F.; Peng, X. G. *Nano Lett.* **2006**, *6*, 720.
(55) Son, J. S.; Wen, X. D.; Joo, J.; Chae, J.; Baek, S. I.; Park, K.; Kim, J. H.; An, K.; Yu, J. H.; Kwon, S. G.; Choi, S. H.; Wang, Z. W.; Kim, Y. W.; Kuk, Y.; Hoffmann, R.; Hyeon, T. *Angew. Chem., Int. Ed.* **2009**, *48*, 6861.
(56) Liu, Y. H.; Wang, F. D.; Wang, Y. Y.; Gibbons, P. C.; Buhro, W. E. *J. Am. Chem. Soc.* **2011**, *133*, 17005.
(57) Rice, K. P.; Saunders, A. E.; Stoykovich, M. P. *J. Am. Chem. Soc.* **2013**, *135*, 6669.
(58) Bala, T.; Prasad, B. L. V.; Sastry, M.; Kahaly, M. U.; Waghmare, U. V. *J. Phys. Chem. A* **2007**, *111*, 6183.
(59) Sung, Y. M.; Park, K. S.; Lee, Y. J.; Kim, T. G. *J. Phys. Chem. C* **2007**, *111*, 1239.
(60) Qin, H. Y.; Niu, Y.; Meng, R. Y.; Lin, X.; Lai, R. C.; Fang, W.; Peng, X. G. *J. Am. Chem. Soc.* **2014**, *136*, 179.
(61) Empedocles, S. A.; Bawendi, M. G. *Science* **1997**, *278*, 2114.

DOI: 10.1021/jacs.6b00674
J. Am. Chem. Soc. 2016, 138, 6475−6483